J|A|C|S ARTICLES

Published on Web 04/08/2009

Light Penetration and Photoisomerization in Rhodopsin studied by Numerical Simulations and Double-Quantum Solid-State NMR Spectroscopy

Maria Concistrè,[†] Axel Gansmüller,[†] Neville McLean,[†] Ole G. Johannessen,[†] Ildefonso Marín Montesinos,[†] Petra H. M. Bovee-Geurts,[‡] Richard C. D. Brown,[†] Willem J. DeGrip,[‡] and Malcolm H. Levitt*,[†]

School of Chemistry, University of Southampton, SO17 1BJ Southampton, U.K., and Nijmegen Centre for Molecular Life Sciences, Radboud University, NL-6500 HB Nijmegen, The Netherlands

Received December 29, 2008; E-mail: mhl@soton.ac.uk

Abstract: The penetration of light into optically thick samples containing the G-protein-coupled receptor rhodopsin is studied by numerical finite-element simulations and double-quantum solid-state NMR experiments. Illumination with white light leads to the generation of the active bathorhodopsin photostate in the outer layer of the sample but generates a large amount of the side product, isorhodopsin, in the sample interior. The overall yield of bathorhodopsin is improved by using monochromatic 420 nm illumination and by mixing the sample with transparent glass beads. The implications of these findings on the interpretation of previously published rhodopsin NMR data are discussed.

1. Introduction

Rhodopsin is a G-protein-coupled receptor (GPCR) responsible for dim light vision in mammals. Rhodopsin consists of seven transmembrane helices, with the 11-Z-retinylidene chromophore covalently bound to the lysine-296 residue via protonated Schiff base (PSB) linkage. Light absorption isomerizes the retinylidene chromophore to form the strained *all-E* intermediate *bathorhodopsin*, which has been studied by X-ray diffraction,[1] femtosecond stimulated Raman spectroscopy,[2,3] and solid-state NMR.[4,5]

At physiological temperatures bathorhodopsin passes spontaneously through a further sequence of intermediates leading eventually to the active-state metarhodopsin-II, which is able to bind and activate many copies of the G-protein transducin. This leads to a change in the transmembrane potential and eventually to the induction of an optic nerve signal.[6] The main species involved in the photocycle of rhodopsin are summarized in Figure 1.

It is possible to trap and study bathorhodopsin by maintaining the sample temperature below 125 K[7,8] during illumination and during the data acquisition process. This has allowed study of the molecular-scale structure of bathorhodopsin by low-temperature X-ray diffraction[1] and of its electronic structure by double-quantum ^{13}C solid-state NMR.[5] However, the clean preparation of bathorhodopsin by illumination at low temperature is made more complicated by (i) the complex photochem-

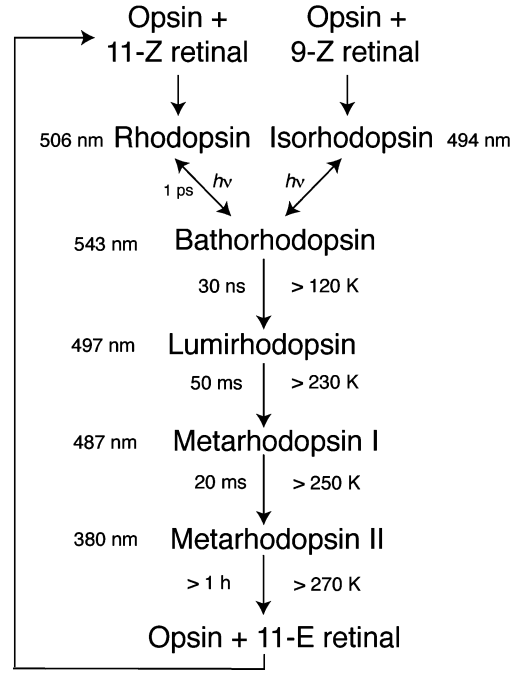

Figure 1. Summary of the rhodopsin photocycle, showing the wavelengths of maximum light absorption, and the temperatures at which each intermediate is stable. The data are adapted from refs 7 and 10

[†] University of Southampton.
[‡] Nijmegen Centre for Molecular Life Sciences.

(1) Nakamichi, H.; Okada, T. *Angew. Chem., Int. Ed.* **2006**, *45*, 4270–4273.
(2) Kukura, P.; McCamant, D. W.; Yoon, S.; Wandschneider, D. B; Mathies, R. A. *Science* **2005**, *310*, 1006–1009.
(3) Yan, E. C. Y.; Ganim, Z.; Kazmi, M. A.; Chang, B. S. W.; Sakmar, T. P.; Mathies, R. A. *Biochemistry* **2004**, *43*, 10867–10876.
(4) Smith, S. O.; Courtin, J.; De Groot, H. J. M.; Gebhard, R.; Lugtenburg, J. *Biochemistry* **1991**, *30*, 7409–7415.
(5) Concistrè, M.; Gansmüller, A.; McLean, N.; Johannessen, O. G.; Marín Montesinos, I.; Bovee-Geurts, P. H. M.; Verdegem, P.; Lugtenburg, J.; Brown, R. C. D.; DeGrip, W. J.; Levitt, M. H. *J. Am. Chem. Soc.* **2008**, *130*, 10490–10491.
(6) Rodieck, R. W. *The First Step in Seeing*; Sinauer Associates, Inc.: Sunderland, MA, 1998.
(7) Palczewski, K. *Annu. Rev. Biochem.* **2006**, *75*, 743–767.
(8) Yoshizawa, T.; Wald, G. *Nature (London)* **1963**, *197*, 1279–1286.

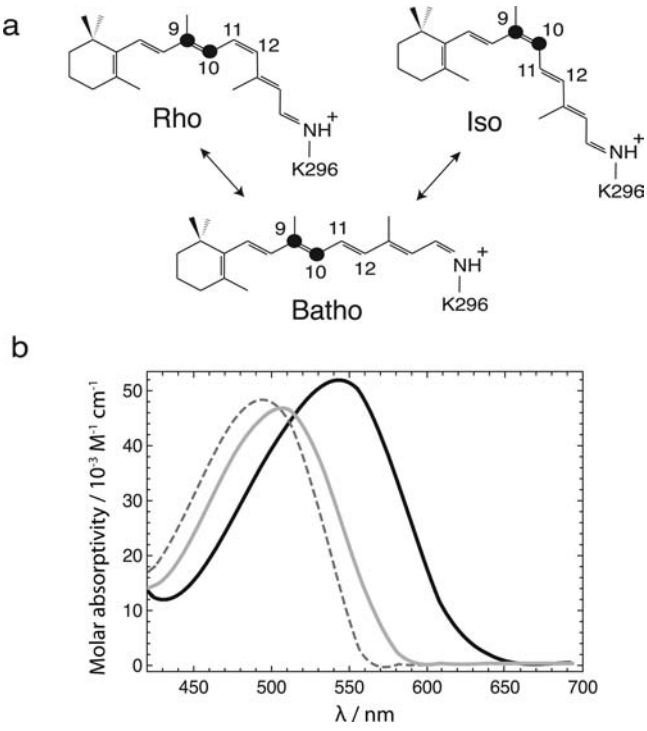

Figure 2. (a) Three rhodopsin isomers involved at temperatures below 150 K. The 9,10-$^{13}C_2$ labels are indicated by filled circles. (b) The optical absorption spectra at $T = 120$ K of the three isomers: rhodopsin (solid gray line), isorhodopsin (broken line), and bathorhodopsin (solid black line). The data are adapted from refs 9 and 10.

istry at the start of the rhodopsin photocycle, and (ii) the limited penetration of light into the sample interior, due to the strong photon absorption by rhodopsin and bathorhodopsin at the surface. The light-penetration issue is particularly important for solid-state NMR studies of rhodopsin photointermediates, which often require relatively thick samples (~1 mm) containing high rhodopsin concentrations in order to achieve sufficiently large NMR signals.

The penetration of light into rhodopsin samples is a complicated process since the photointermediate composition of the outer layers affects the penetration of light into the sample interior. The composition of photoisomers is therefore a function of time, space, and photon wavelength distribution. As shown in Figure 2, the distorted *all-E* chromophore of bathorhodopsin may itself be photoisomerized, leading to either the starting 11-Z state rhodopsin, or the 9-Z side product isorhodopsin.[9] The three species have different optical absorption spectra, as sketched in Figure 2. The absorption maximum of ground-state rhodopsin is at 506 nm, while bathorhodopsin has a red-shifted absorption maximum at 543 nm, and isorhodopsin has a blue-shifted absorption maximum at 494 nm.[10] Furthermore, absorption of light by isorhodopsin may in turn lead to the regeneration of bathorhodopsin. The absorption spectra and wavelength-dependent quantum yields of the three molecules rhodopsin, bathorhodopsin, and isorhodopsin have been thoroughly documented.[8−10]

Many early NMR studies of rhodopsin photointermediates did not pay much attention to the issue of light penetration and the possible generation of multiple photoisomers. For example, several studies of the photostate *metarhodopsin-I* used illumination of rhodopsin by white light under cryogenic conditions, followed by warming to 250 K, to trap the *metarhodopsin-I* photostate.[11,12] However, as shown below, these conditions are much more likely to accumulate the photostate *isorhodopsin* rather than *metarhodopsin-I*. This calls into question some of the conclusions of those reports.

In the current work we employ two techniques in parallel to study light penetration and photoisomerization in optically dense rhodopsin samples, and to optimize the conditions for the study of the functionally relevant *bathorhodopsin* photostate. First, we performed finite-element numerical simulations to predict the accumulation of the isorhodopsin and bathorhodopsin photoisomers in cold illuminated samples, as a function of time, space, rhodopsin concentration, illumination intensity, and light wavelength distribution. Second, we validated the results of these simulations by using double-quantum ^{13}C solid-state NMR of rhodopsin labeled with ^{13}C at positions 9 and 10 of the retinylidene prosthetic group. Solid-state NMR can follow the photoisomerization process in thick samples since each photoisomer has a set of characteristic ^{13}C chemical shifts and the samples are almost completely transparent to radiowaves. The balance of photoisomers is therefore probed in the interior of the sample, rather than at the surface, in contrast to optical studies.

Our results show that the optimal illumination conditions for generation of bathorhodopsin are quite different in optically thin and optically thick samples. In the case of optically thin samples, the yield of bathorhodopsin is relatively insensitive to the wavelength distribution of the visible light. However, in the case of samples thicker than a few tens of micrometers, the wavelength distribution of the incident light has a strong influence on the bathorhodopsin yield. Long-wavelength components in the light destroy bathorhodopsin and cause the accumulation of isorhodopsin, which is usually an unwanted side product. In samples with rhodopsin concentrations of around 6 mM, bathorhodopsin cannot be generated at depths greater than about 400 μm in a reasonable amount of time, however strong is the light and whatever its wavelength. This conclusion guided the development of a new protocol for improving the yield of bathorhopsin, in which the rhodopsin is mixed with small glass beads to increase the illuminated surface area. This method led to the successful characterization of bathorhodopsin by solid-state NMR.[5] In this paper we provide the theoretical background and numerical simulations underlying this protocol, and show experimental NMR results.

2. Methods

2.1. Simulations of Light Penetration and Photoisomerization. Consider a sample of lipids loaded with rhodopsin, with the initial rhodopsin concentration denoted c_R^0. Photons with a distribution of wavelengths λ impinge on the surface, which is assumed to be flat. The photons penetrate the sample and induce photoisomerization between the three forms rhodopsin, bathorhodopsin, and isorhodopsin. If the temperature is low enough and all side reactions are ignored, the concentrations of the three photoisomers vary as a

(9) Birge, R. R.; Einterz, C. M.; Knapp, H. M.; Murray, L. P. *Biophys. J.* **1988**, *53*, 367–385.
(10) Yoshizawa, P.; Shichida, Y.; Matuoka, S. *Vision. Res.* **1984**, *24*, 1455–1463.
(11) Feng, X.; Verdegem, P. J. E.; Eden, M.; Sandstrom, D.; Lee, Y. K.; Bovee-Geurts, P. H. M.; de Grip, W. J.; Lugtenburg, J.; De Groot, H. J. M.; Levitt, M. H. *J. Biomol. NMR* **2000**, *16*, 1–8.
(12) Verdegem, P. J. E.; Bovee-Geurts, P. H. M.; de Grip, W. J.; Lugtenburg, J.; de Groot, H. J. M. *Biochemistry.* **1999**, *38*, 11316–11324.

function of time and depth z below the surface, such that the total concentration of rhodopsin isomers is constant, i.e.

$$c_R(z,t) + c_B(z,t) + c_I(z,t) = c_R^0 \tag{1}$$

The simulations may predict the dependence of the three concentrations on depth z and time t, and thereby provide insight into the optimal conditions for the preparation of bathorhodopsin.

Denote the incident photon flux density (number of photons per unit time and unit area, at a given wavelength λ) by I_λ^0. Illumination with a mixture of wavelengths is taken into account by defining an incident photon flux vector as follows:

$$\mathbf{I}^0 = \begin{pmatrix} I_{\lambda_1}^0 \\ I_{\lambda_2}^0 \\ \vdots \end{pmatrix} \tag{2}$$

In the simulations described below, the effect of white illumination is emulated by employing photons with five different colors.

Consider a small volume element $\delta V = A\delta z$, with surface area A, located at depth z below the illuminated surface (defined to be at $z = 0$), and with a thickness δz (assumed to be small enough that there is negligible change in light intensity while traversing the slice). Denote the concentrations of rhodopsin, bathorhodopsin, and isorhodopsin in this volume element at a given time t by a 3-vector:

$$\mathbf{c}(z,t) = \begin{pmatrix} c_R(z,t) \\ c_B(z,t) \\ c_I(z,t) \end{pmatrix} \tag{3}$$

The absorption coefficients of the three relevant species are given in the literature over a range of wavelengths.[9] These coefficients may be collated by defining an extinction coefficient matrix:

$$\varepsilon = \begin{pmatrix} \varepsilon_R(\lambda_1) & \varepsilon_R(\lambda_2) & \vdots \\ \varepsilon_B(\lambda_1) & \varepsilon_B(\lambda_2) & \vdots \\ \varepsilon_I(\lambda_1) & \varepsilon_I(\lambda_2) & \vdots \end{pmatrix} \tag{4}$$

The rows of the matrix define the properties of individual photoisomers, while the columns of the matrix indicate the photon wavelengths. The simulations described here use the following matrix:

$$\varepsilon = \begin{pmatrix} 14.2 & 40.9 & 43.7 & 6.1 & 1.0 \\ 12.4 & 30.0 & 47.8 & 46.4 & 30.0 \\ 17.9 & 46.9 & 36.2 & 0.6 & 0.1 \end{pmatrix} \times 10^3\ \mathrm{M^{-1}\ cm^{-1}}$$

where the columns refer to light wavelengths of 420, 479, 520, 565, and 620 nm, respectively, and the rows correspond to rhodopsin, bathorhodopsin, and isorhodopsin. These parameters are taken directly from ref 9 except for the 420 nm data, which was estimated from published absorption curves.[10] Note that bathorhodopsin has the strongest absorption at long wavelengths, while isorhodopsin has the strongest absorption at short wavelengths (see Figure 2b).

Denote the flux density for photons of wavelength λ impinging on the surface of the volume element δV at time t by $I_\lambda(z,t)$. These photons may either be transmitted through the slice, or absorbed by one of the photoisomers. The photon flux illuminating a slice at depth z and time t at a set of different wavelengths is given by the column vector $\mathbf{I}(z,t)$ as follows:

$$\mathbf{I}(z,t) = \begin{pmatrix} I_{\lambda_1}(z,t) \\ I_{\lambda_2}(z,t) \\ \vdots \end{pmatrix} \tag{5}$$

First consider the transmission of light from one slice to the next. From the Beer−Lambert law, the numbers of photons at each wavelength λ absorbed by *all* photoisomers at depth z per unit time are given by the elements of the following vector:

$$\mathbf{I}^{\mathrm{abs}}(z,t) = \mathbf{c}(z,t)^{\mathrm{T}} \cdot \varepsilon \cdot \mathrm{I}(z,t)\delta z \times \ln 10 \tag{6}$$

where the factor ln 10 is required by the conventional definition of the absorption coefficient, and the superscript T indicates a transpose. If one assumes that all photons are either absorbed or transmitted (neglecting reflection and scattering), the wavelength-dependent photon flux impinging on the *next* slice is given by

$$\mathbf{I}(z+\delta z, t) = \mathbf{I}(z,t) - \mathbf{I}^{\mathrm{abs}}(z,t) \tag{7}$$

At each point in time, the photon flux inside the sample may be calculated by applying eqs 6 and 7 to successively deeper sample layers, providing that the spatially dependent isomer concentrations $\mathbf{c}(z,t)$ are known.

Now consider an individual rhodopsin molecule located in the volume element δV at time t. The probability of this molecule absorbing a photon of any wavelength during the time interval δt is given by

$$p_R^{abs}(z,t) = \ln 10 \times \sum_\lambda \varepsilon_R(\lambda) I_\lambda(z,t)\delta t \tag{8}$$

Hence, the concentration of rhodopsin molecules absorbing photons in the volume element δV during the time interval δt is given by

$$c_R^{abs}(z,t) = p_R^{abs}(z,t) c_R(z,t) = \ln 10 \times \sum_\lambda \varepsilon_R(\lambda) c_R(z,t) I_\lambda(z,t)\delta t \tag{9}$$

This calculation may be repeated for the two other photoisomers leading to the elements of the vector $\mathbf{c}^{abs}(z,t)$, which represents the concentration of molecules of each photoisomer absorbing light in the volume element δV during the time interval δt:

$$\mathbf{c}^{abs}(z,t) = \ln 10 \times \sum_\lambda \begin{pmatrix} \varepsilon_R(\lambda) c_R(z,t) \\ \varepsilon_B(\lambda) c_B(z,t) \\ \varepsilon_I(\lambda) c_I(z,t) \end{pmatrix} I_\lambda(z,t)\delta t \tag{10}$$

When a photon is absorbed, it may lead to either a photoisomerization process or regeneration of the initial state. The probabilities of these processes are summarized by a *quantum yield matrix*, denoted Φ, which is defined as follows:

$$\Phi = \begin{pmatrix} \Phi_{RR} & \Phi_{RB} & \Phi_{RI} \\ \Phi_{BR} & \Phi_{BB} & \Phi_{BI} \\ \Phi_{IR} & \Phi_{IB} & \Phi_{II} \end{pmatrix} \tag{11}$$

where for example the element Φ_{BR} indicates the probability that a photoexcited rhodopsin molecule generates a bathorhodopsin molecule (the subscripts should be read from right to left). Diagonal elements such as Φ_{RR} indicate the probability that a rhodopsin molecule, having absorbed a photon, simply returns to its initial state. All columns sum to unity, corresponding to the assumption that absorption of a photon always leads to either no isomerization at all, or to generation of one of the two specified photoisomers, with no side-reactions. The quantum yields are documented in the literature[8,9] and are wavelength-dependent. In practice, we used the following matrix:

$$\Phi = \begin{pmatrix} 0.33 & 0.33 & 0 \\ 0.67 & 0.60 & 0.16 \\ 0 & 0.07 & 0.84 \end{pmatrix} \tag{12}$$

This is adapted from the published 77 K data in refs 8, 9 ignoring the temperature- and wavelength-dependence of the quantum yields, for the sake of simplicity. The very small wavelength-dependence of the largest quantum yield $\Phi_{BR} = 0.67$ has been confirmed experimentally.[9] Note that both rhodopsin and isorhodopsin may be isomerized directly to bathorhodopsin, but not to each other. In addition, note that rhodopsin is isomerized to bathorhodopsin with approximately twice the efficiency of isorhodopsin. The very high

quantum yield for conversion of rhodopsin to bathorhodopsin ($\Phi_{BR} = 0.67$) is the focus of much research and experimental study.[2,3] There is evidence that this high quantum yield is due in part to interactions with the protein binding pocket, which prepares the retinylidene chain in a conformation characterized by favorable single-bond torsional twists.[2,3]

The changes in the three photoisomer concentrations at depth z during a small time interval δt are therefore given by the following vector:

$$\delta \mathbf{c}(z,t) = \Phi \cdot \mathbf{c}^{abs}(z,t)\delta t \tag{13}$$

Equations 10 and 13 relate the change in the isomer concentrations to the penetration of light, while eqs 6 and 7 relate the penetration of light to the isomer concentrations.

The changing profiles of photoisomer concentrations may therefore be predicted by numerical integration of these equations using the boundary conditions of a constant light flux density at the sample surface, and a starting state of no photoisomerization:

$$I_\lambda(0,t) = I_\lambda^0 \text{ independent of } t$$
$$\mathbf{c}(z,0) = \begin{pmatrix} c_R^0 \\ 0 \\ 0 \end{pmatrix} \text{ independent of } z \tag{14}$$

where c_R^0 is the initial rhodopsin concentration. Incident light with different spectral characteristics may be simulated by using incident photon flux densities I_λ^0 for several different wavelengths.

The dynamical equations were integrated by finite-element numerical simulations using about 100 volume elements and 5000 time increments. The thickness of the volume elements and the length of the time intervals were chosen to be small enough to provide an accurate integration of the differential equations. Convergence of the integration was tested by showing that the simulation results were insensitive to further reductions in the size of the time or volume elements. For the 420 nm simulations, the element thickness was 10 μm, and the time increment was 20 s. For the white-light simulations, the element thickness was 1 μm, and the time increment was 5 s. The starting concentration of rhodopsin was $c_R^0 = 5.8$ mM, corresponding to the typical concentration of our sample preparations.

2.2. Sample Preparation. The doubly ^{13}C-labeled chromophore ([9,10-$^{13}C_2$]-retinal) was prepared by organic synthesis as described in the Supporting Information of ref 13. The bovine rhodopsin sample was prepared as described in ref 14. Labeled 11-Z-retinal was incorporated into the purified protein opsin, followed by reconstitution in the natural membrane lipids. The purity of the 11-Z retinal was at least 90%. Minor contamination by *all-trans* retinal or 13-Z-retinal, should not interfere with these measurements, since they would not bind to opsin. If present in small quantities as retinaloximes left over from the regeneration stage, their ^{13}C peaks would be spectrally distinct, and they would not respond to the illumination since their absorption is very low at wavelengths greater than 420 nm. In practice no such impurity peaks were observed. Contamination with 9-Z-retinal was also negligible, since this would react with opsin to generate isorhodopsin and the corresponding ^{13}C peaks were not observed in the spectra before illumination. The efficiency of incorporation of the 11-Z retinal in opsin is more than 90% and the efficiency of reconstitution of rhodopsin into proteoliposomes is about 99%. The A_{280}/A_{520} values of the reconstituted preparations are 2.0 ± 0.1. The resulting rhodopsin concentration was ~ 5.8 mM. The sample was stored at 193 K and was always handled in the dark or under dim red light. The rhodopsin/lipid samples were frozen with liquid nitrogen and ground using a cold mortar and pestle to form particles of size ~100 μm.

2.3. Low-Temperature Magic-Angle Spinning. All NMR experiments were performed at a sample temperature of 120K using magic-angle spinning (MAS) with a spinning frequency of $\omega_r/2\pi = 7.00$ kHz ± 50 Hz. The sample was contained in a thin-wall zirconia rotor with outer diameter 4 mm and wall thickness 0.55 mm. A sapphire rotor was tested but found to be unsuitable for these experiments. Although sapphire allows much more light to reach the sample, its high thermal conductivity at low temperatures makes it more difficult to reach the required sample temperature of 120 K. This is because the nitrogen gas bearings have to be kept relatively warm in order to avoid spinning instabilities, since the viscosity and the density of nitrogen gas are strong functions of temperature near its boiling point. Under these conditions, the high thermal conductivity of sapphire conducts heat efficiently from the relatively warm bearing region into the sample chamber. As a result, we found that sufficiently low sample temperatures could not be attained by using a sapphire rotor. In principle, sapphire rotors could be used in conjunction with cold helium as the bearing gas, but this would require a considerable redesign and additional expense.

The low sample temperature was achieved by continuously exposing the sample container (rotor) to a thermostatted flow of dry nitrogen gas precooled by passing through a bath of liquid nitrogen (77 K). The bearing and drive gas flows used to support and propel the rotor were brought into thermal contact with the cooling gas in order to reduce temperature gradients. All N_2 gas flows were generated by a dedicated liquid N_2 evaporation facility. As discussed in the Supporting Information of ref 5, the temperature inside the NMR rotor is a function of the nitrogen gas temperature, nitrogen gas flow, and the spinning frequency. A precise calibration of the temperature inside the sample was achieved by measuring the ^{207}Pb signal of $Pb(NO_3)_2$, for which the ^{207}Pb chemical shift is known to be temperature dependent.[15,16] Details and experimental procedures used for the temperature calibration are reported in the Supporting Information of ref 5. When spinning at 7 kHz MAS we observed discrepancies up to 50 °C between the cooling gas and the real sample temperature, as well as temperature gradients of up to 25 °C inside the rotor. Care was taken to keep the warmest part under 120 K throughout the experiments, in order to ensure that rhodopsin, bathorhodopsin, and isorhodopsin are the only photointermediates present in significant concentrations. These observations stress the importance of generating the photointermediates *in situ* under conditions allowing proper calibration of the true sample temperature.

2.4. Illumination. The sample was illuminated inside the NMR rotor by using two light sources, each comprising a 250 W quartz halogen lamp, a filter, and a lens, with a custom-built housing designed to protect the optical fibers from thermal damage. The light from each lamp was passed through a cooled interference filter, to select the appropriate wavelength and suppress infrared components, and was focused onto the polished ends of an optical fiber bundle. A total of 14 optical fibers were used, directed onto the outside of the sample rotor from a variety of angles. Three different sets of optical interference filters were used. Two band-pass filters centered on $\lambda = 480 \pm 5$ nm and 420 ± 5 nm and a low-pass filter with $\lambda \leq 495$nm. All filters and lenses were supplied by Edmund Optics (York, U.K.).

In the case of a narrow-band interference filter, an optical power output of 30 μW was measured at the end of each fiber by using an optical power meter (Newport, U.S.A.). The attenuation of the light by the rotor walls (0.55 mm wall thickness) was measured to be around 90%. The total light power at the sample surface from all 14 fibers was therefore estimated to be about $P \simeq 42$ μW, for the case of narrowband filtered light.

The estimated light power P at a single wavelength λ may be converted into a photon flux estimate by using the formula $I_\lambda^0 =$

(13) Lai, W. C.; et al. *J. Am. Chem. Soc.* **2006**, *128*, 3878–3879.
(14) De Grip, W. J.; Daemen, F. J. M.; Bonting, S. L. *Methods Enzymol.* **1980**, *67*, 301–320.
(15) Bielecki, A.; Burum, A. *J. Magn. Reson. A* **1995**, *116*, 215–220.
(16) Beckmann, P. A.; Dybowski, C. *J. Magn. Reson.* **2000**, *146*, 379–380.

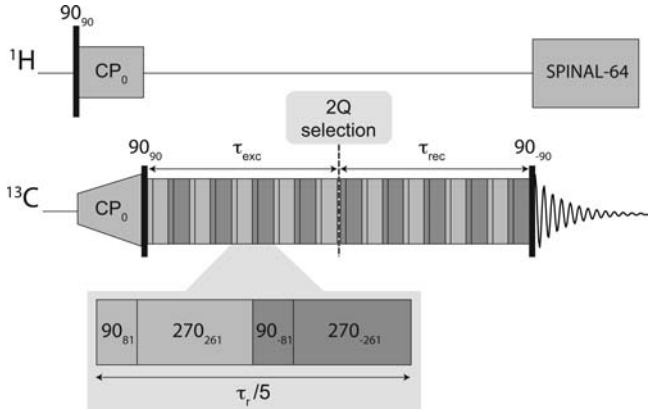

Figure 3. Double quantum dipolar recoupling sequence used to select NMR signals from pairs of ^{13}C enriched nuclear resonances in rhodopsin samples. Pulse flip angles and radio frequency phases are given in degrees.

$P\lambda/hcA$ where A is the illuminated area. In the present case the illuminated area is estimated to be $A \simeq 182 \times 10^{-6}$ m^2, using a sample radius of 1.45 mm and length 20 mm. This leads to an estimated photon flux at the sample surface of $I_\lambda^0 \simeq 0.75$ μmol m^{-2} s^{-1} for a wavelength of 420 nm.

2.5. Double-Quantum Solid-State NMR. Observation of the ^{13}C NMR signals from the $^{13}C_2$-labeled chromophore requires suppression of the dominant signals from natural-abundance ^{13}C nuclei in the protein and lipid matrix. This was done by using the double-quantum-filter pulse sequence shown in Figure 3. After cross-polarization of ^1H magnetization to ^{13}C, double-quantum ^{13}C coherence was excited by using a $R20_2^9$ symmetry-based recoupling sequence constructed as follows:

$$R20_2^9 = \hat{G}_{\mathrm{rep}}(10) * \hat{G}_\sigma(2) * \hat{\Phi}\left(\frac{9\pi}{20}\right) \cdot (90_0 270_{180})$$

where the cycle duration is two rotor periods and the notation is defined in ref 17. The radiofrequency phases in the recoupling sequence are shown explicitly in Figure 3. The double-quantum excitation and reconversion periods were equal, with a value optimized experimentally to give the maximum double-quantum-filtered signal ($\tau_{\mathrm{exc}} = \tau_{\mathrm{rec}} = 400$ μs). No decoupling was performed on the ^1H channel during the $R20_2^9$ double-quantum recoupling sequence.[18] ^1H decoupling during the acquisition of the ^{13}C free-induction decay was achieved using a Small Phase INcremental ALternation with 64 steps (SPINAL-64 sequence)[19] with a ^1H rf nutation frequency of 80 kHz and a pulse length of 6.3 μs. Signals passing through double-quantum ^{13}C coherence were selected by using a standard phase cycle of 16 steps. The double-quantum-filtering efficiency (as compared to a cross-polarization experiment without double-quantum filtration) was around 35%. The selection of the $^{13}C_2$-labeled chromophore signals was usually excellent, although weak residual signals at the positions of the strong protein and lipid peaks could sometimes be observed. The amplitudes of the residual signals were consistent with them being due to naturally occurring $^{13}C_2$ pairs.

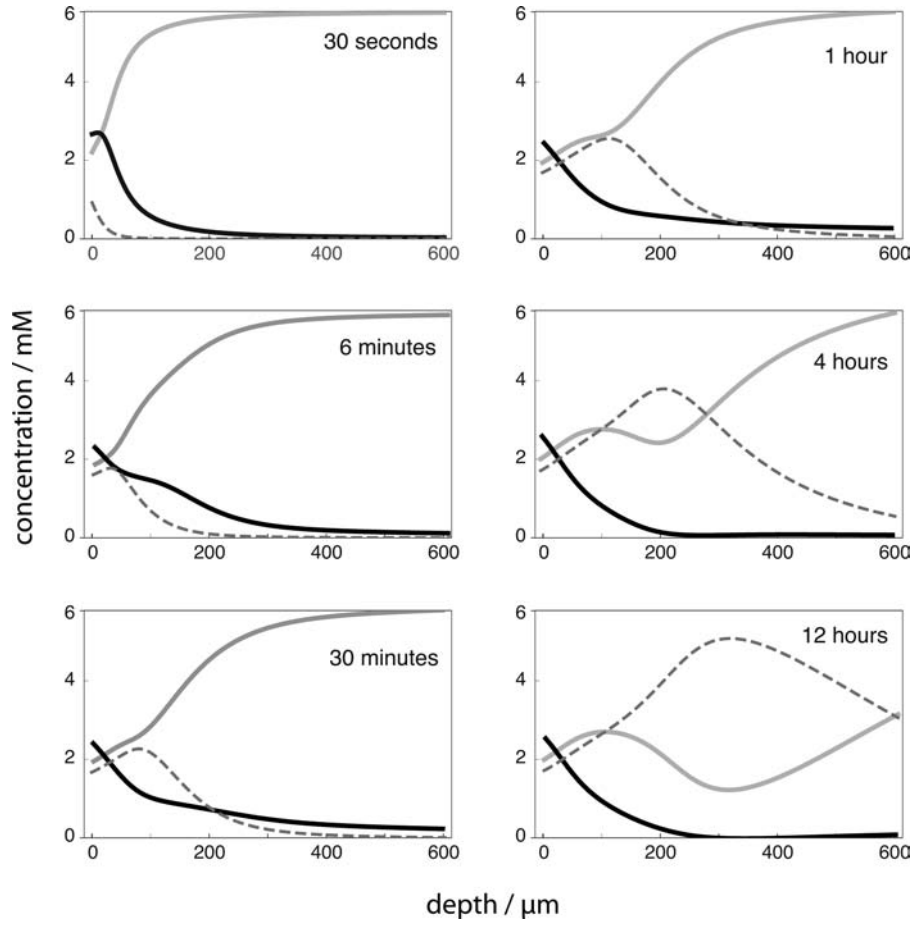

Figure 4. Finite-element numerical simulations of photoisomerization in a sample containing 5.8 mM of rhodopsin, exposed to white light. Photon fluxes of 0.75 μmol m^{-2} s^{-1} for each of the five wavelengths 420 nm, 479 nm, 520 nm, 565 and 620 nm are applied to the surface of the sample (left-hand edge of the plots). The plots show the simulated concentrations of rhodopsin (solid gray line), bathorhodopsin (solid black line) and isorhodopsin (broken line) at the indicated times, as a function of depth below the surface (horizontal axis). Note the rapid generation of bathorhodopsin in a thin surface layer followed by the strong accumulation of isorhodopsin deeper in the sample at long times.

The NMR spectra shown in this paper result from summing together around 10^4 NMR signal transients, each separated by 5 s for thermal equilibration of the nuclear spin magnetization. Each spectrum required about 17 h of data acquisition.

3. Results

The ^{13}C chemical shifts of the C10 retinylidene site are clearly distinguishable for rhodopsin, isorhodopsin, and bathorhodopsin. Double-quantum-filtered ^{13}C MAS NMR of [9,10-$^{13}C_2$]-retinylidene-labeled rhodopsin may therefore be used to assess the distributions of these photostates in optically dense samples. In this section, numerical simulations of the light penetration and photoisomerization are compared with experimental solid-state NMR data, for two different illumination scenarios.

3.1. White Light Illumination.

3.1.1. Numerical Simulations. Figure 4 shows numerical photoisomerization simulation results for a simple model of white light. The incident photon fluxes were set to $I_\lambda^0 = 0.75$ μmol m^{-2} s^{-1} for each of the five wavelengths 420, 479, 520, 565, and 620 nm. The concentrations of rhodopsin, bathorhodopsin, and isorhodopsin are shown by a solid gray line, a solid black line, and a dashed line, respectively. The initial impact of the white light (top left panel) is to isomerize about half of the rhodopsin in a $\sim$40 μm surface layer to bathorhodopsin. Lower layers are not affected in the initial stages since the light penetration is blocked by the rhodopsin nearer the surface. After a few minutes of illumination, bathorhodopsin starts to build up at a depth of about $\sim$150 μm. However, as the illumination continues, the build-up of bathorhodopsin is reversed in favor of a strong accumulation of the isorhodopsin photoisomer. At long times, most of the interior of the sample is converted to isorhodopsin, with bathorhodopsin still confined to a $\sim$40 μm surface layer.

This behavior is due to the different absorption characteristics and quantum yields of the three photoisomers. The behavior in the outer layers of the sample, where light is abundant, is dominated by the quantum yields. Rhodopsin has a large quantum yield for conversion to bathorhodopsin, and hence, bathorhodopsin is favored in this region. However, deeper into the sample, the penetration of light is the dominating factor. All three photoisomers absorb strongly at medium-to-short wavelengths, so only long-wavelength red/orange light penetrates to large depths. The rhodopsin and bathorhodopsin photoisomers absorb red more strongly than isorhodopsin. Although bathorhodopsin has a low quantum yield for conversion to isorhodopsin, any isorhodopsin that is formed deep in the sample by photoisomerization of bathorhodopsin remains in that form since isorhodopsin is almost transparent to red light. Furthermore, the conversion of the other isomers into isorhodopsin renders the sample even more transparent to red light, so the conversion process can now proceed at greater depths than before. As a result, isorhodopsin accumulates in the sample interior. A wave of isorhodopsin propagates into the sample, as can be clearly seen in the right-hand panels of Figure 4 (dashed lines).

3.1.2. NMR Results. Figure 5a shows a double-quantum-filtered (DQF) spectrum of [9,10-^{13}C]-retinylidene rhodopsin before illumination. The chemical shifts of the two peaks in the spectrum (148.9 ppm for C9 and 127.9 ppm for C10) agree with the values obtained in previous studies.[20]

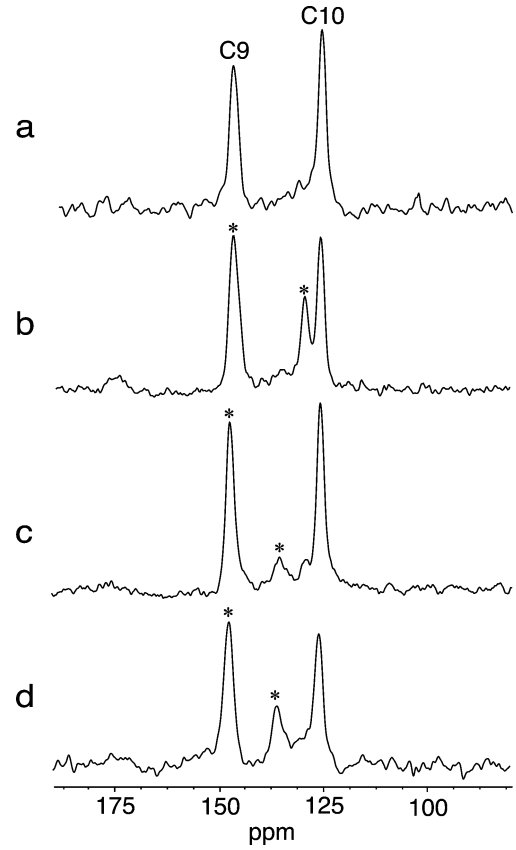

Figure 5. Double-quantum filtered ^{13}C NMR spectra of [9,10-^{13}C]-retinylidene rhodopsin:(a) before illumination (12k transients); (b) after 12 h of illumination under white light (8k transients); (c) after 12 h of illumination with 420 ± 5 nm light (12k transients); (d) after 12 h of illumination with 420 ± 5 nm light on an homogeneous mixture of rhodopsin and glass beads (12k transients). All spectra were acquired at a temperature $<$120 K with magic-angle spinning at 7.00 ± 0.05 kHz. All chemical shifts are referenced indirectly to TMS using the rhodopsin shift data in ref 20. The positions of the new signals are indicated by asterisks.

Figure 5b shows a DQF spectrum of [9,10-^{13}C]-retinylidene rhodopsin acquired after 12 h of illumination under white light. The retinylidene-C10 rhodopsin peak is reduced in intensity and a strong new peak appears at 131.4 ppm. This is attributed to the retinylidene-C10 site of isorhodopsin, in agreement with previous isorhodopsin data.[21] In addition, the low-field peak becomes slightly broader after illumination (increase in line width from 220 to 265 Hz). This is also consistent with the formation of isorhodopsin, since the retinylidene-C9 peak of isorhodopsin is at 148.2 ppm.[21]

The generation of a large isorhodopsin fraction by white light illumination is in qualitative agreement with the simulations of light penetration and photoisomerization, described above. Note, however, that a *quantitative* correspondence cannot easily be made between the illumination simulations and the NMR results, since the NMR spectra are integrals over the entire sample volume.

(17) Levitt, M. H. *J. Chem. Phys.* **2008**, *128*, 52205–52225.
(18) Marin-Montesinos, I.; Brouwer, D.; Antonioli, G. C.; Lai, W. C.; Levitt, M. H. *J. Magn. Reson.* **2005**, *177*, 307–317.
(19) Fung, B. M.; Khitrin, A. K.; Ermolaev, K. *J. Magn. Reson.* **2000**, *142*, 97–101.
(20) Creemers, A.; Kiihne, S.; Bovee-Geurts, P. H. M.; de Grip, W. J.; Lugtenburg, J.; de Groot, H. J. M. *Proc. Natl. Acad. Sci. U.S.A.* **2002**, *99*, 9101–9106.
(21) Creemers, A.; Bovee-Geurts, P.; De Grip, W. J.; Lugtenburg, J.; De Groot, H. J. M. *Biochemistry* **2004**, *43*, 16011–16018.

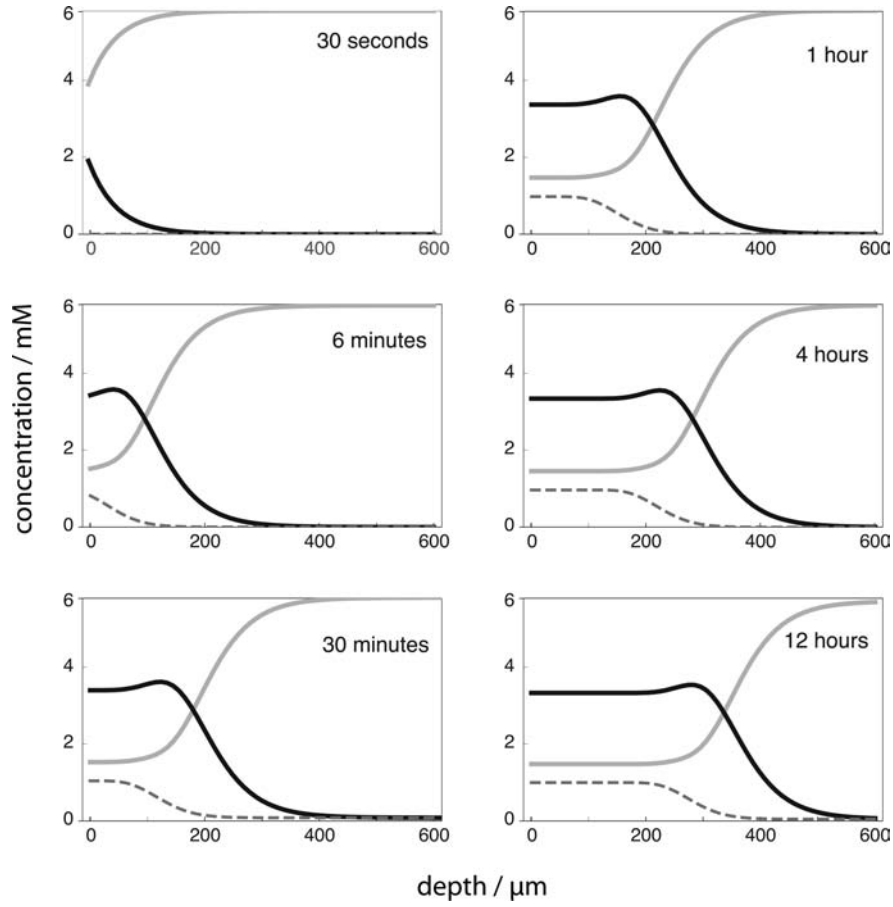

Figure 6. Finite-element numerical simulations of photoisomerization in a sample containing 5.8 mM of rhodopsin, exposed to 0.75 μmol m^{-2} s^{-1} of monochromatic 420 nm light. The plots show the simulated concentrations of rhodopsin (solid gray line), bathorhodopsin (solid black line) and isorhodopsin (broken line) at the indicated times, as a function of depth below the surface (horizontal axis).

3.2. Monochromatic 420 nm Illumination.

3.2.1. Numerical Simulations. The numerical simulations in Figure 6 show how the isomer concentration profiles are predicted to change in time when the sample is illuminated with monochromatic violet light. The photon flux at 420 nm is assumed to be $I^0_{420} = 0.75$ μmol m^{-2} s^{-1}, with all other photon fluxes set to zero.

The immediate impact of the illumination is to isomerize the outer rhodopsin layer to bathorhodopsin, with an efficiency of about 50%. Isorhodopsin is barely formed at all at short times, since bathorhodopsin absorbs short wavelengths inefficiently, and the quantum yield for conversion of bathorhodopsin to isorhodopsin is low.

At longer times a thicker layer of the sample is isomerized, generating an outer layer of mixed bathorhodopsin and isorhodopsin in a ratio of about 10:1. However the advance of the isomerization front progressively slows down as time goes on. After about 12 h of illumination, a layer of thickness ~300 μm is isomerized.

The filled symbols in Figure 7 show the depth of the isomerization front as a function of time, as derived from the numerical simulation results. The front advances rapidly in the initial phase but the advance becomes very slow once the critical depth of about ~300 μm is reached. The progress of the front beyond this point is well-described by a power law of the form $z = at^{\alpha}$, where the exponent $\alpha = 0.184$ was determined by fitting the simulation results at long times (solid line in Figure 7). This weak exponent indicates that it is impractical to thicken the isomerization layer by extending the illumination time. For example, doubling the thickness of the isomerization layer would require a 40-fold increase in the illumination time.

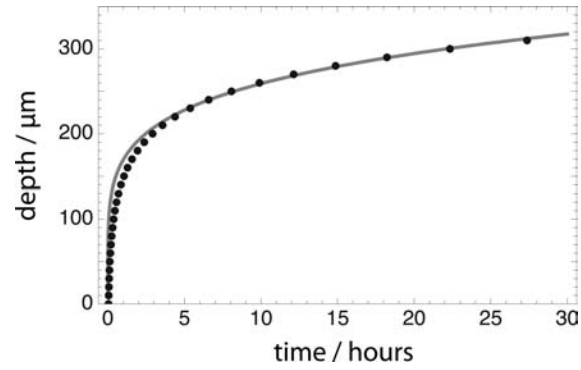

Figure 7. Depth of the isomerization front as a function of time for 5.8 mM of rhodopsin, exposed to 0.75 μmol m^{-2} s^{-1} of monochromatic 420 nm light. The isomerization front is defined here by the position at which the concentration of bathorhodopsin falls below 2.9 mM. The filled symbols indicate the isomerization front positions, derived by numerical simulations. The solid line is a fit of the later time points to the form $z = at^{\alpha}$, where the best-fit exponent is $\alpha = 0.184$.

Further simulations show that increasing the light intensity does not thicken the isomerization layer, but simply speeds up the process of attaining the ~300 μm limit. A decrease in the concentration of the chromophores does not help either. Although the isomerization layer becomes deeper in this case,

the layer still contains the same number of isomerized molecules as before, since the chromophores are more dilute.

3.2.2. NMR Results. Figure 5c shows a DQF ^{13}C spectrum acquired after 12 h illumination of a sample of [9,10-^{13}C]-retynilidene-rhodopsin using a band-pass filter with $\lambda = 420 \pm 5$ nm. A small new peak appears at 137.3 ppm, as well as an even smaller peak at 131.4 ppm which is assigned to the C10 site of isorhodopsin, as described above. The 137.3 ppm peak disappears, to be replaced by a broader and less distinct feature, when the sample temperature was raised above 130 K for about 30 min, before cooling again and acquiring the NMR data. This behavior is consistent with its attribution to bathorhodopsin. However, it is not clear from the spectrum in Figure 5c whether the 137.3 ppm peak belongs to the C9 or C10 site.

The small intensity of the bathorhodopsin peak is consistent with the high molar extinction coefficient of rhodopsin that, as discussed above, only allows a $\sim$300 μm outer layer of the sample to be reached by the light.

We improved the penetration of light into the interior of the sample, and hence the yield of bathorhodopsin, by mixing the rhodopsin-rich particles with $\sim$100 μm diameter glass beads (Sigma-Aldrich). The bead dimensions approximately match the size of the rhodopsin/lipid particles, as estimated by light microscopy. The dispersed glass beads act as light guides, conducting the photons into the interior of the sample, and increasing the proportion of rhodopsin close to an illuminated surface. The sample morphology is a crude mimic of the membrane disk assemblies which are present in rod cells and which perform a similar function.

The following procedure was used to prepare the mixed rhodopsin/lipid/glass bead samples: 34 mg of glass beads (about one-third of the final sample mass) were washed with a buffer solution; 60 mg of the reconstituted [9,10-^{13}C]-retinylidene rhodopsin/lipid mixture was frozen in liquid N_2 and placed with the glass beads in a precooled (193 K) aluminum mortar. The mixture was ground together using a cold pestle and packed into a 4 mm thin-wall zirconia magic-angle-spinning rotor. All procedures were performed in dim red light.

The double-quantum filtered ^{13}C spectrum of the rhodopsin/glass bead mixture, obtained after 12 h of illumination using the $\lambda = 420 \pm 5$ nm band-pass filter, is shown in Figure 5d. As expected, the 137.4 ppm peak, attributed to bathorhodopsin, is much larger than that in Figure 5c. The clear decrease in intensity of the 127.9 ppm retinylidene-C10 peak in Figure 5d indicates that the 137.4 ppm peak should be assigned to the retinylidene-C10 site of bathorhodopsin. The C9 peak of rhodopsin at 148.9 ppm is unchanged, which indicates that the retinylidene-C9 site of bathorhodopsin and rhodopsin have very close ^{13}C chemical shifts, that are not spectrally resolved.

NMR spectra of several other $^{13}C_2$-labeled bathorhodopsin isotopomers were obtained using a similar protocol and are reported in ref 5.

4. Discussion

The penetration of light into optically dense rhodopsin samples is a complex phenomenon since the photoisomerization itself changes the optical characteristics of the illuminated sample layers. In this article we show that this process may be understood with the help of finite-element numerical simulations, and validated by double-quantum solid-state NMR measurements.

In optically thin rhodopsin samples, such as found in the mammalian eye, white light illumination rapidly generates a large fraction of the bathorhodopsin photostate. Under physiological conditions, the bathorhodopsin undergoes rapid thermal isomerization from lumirhodopsin to metarhodopsin-I and to the active state metarhodopsin-II which binds and activates the G-protein transducin. The 9-Z isomer isorhodopsin is unimportant in this context since the quantum yield for isomerization of bathorhodopsin to isorhodopsin is low, and isorhodopsin has nowhere to go except to be isomerized back to bathorhodopsin.

In the optically thick samples which are often used for scientific investigations of molecular structure and function, isorhodopsin may play a much more prominent, and potentially misleading role. In optically thick samples, the wavelength-dependent penetration of light is crucial. White light leads to an accumulation of isorhodopsin in the interior of the sample since it is more transparent to the long wavelengths which penetrate well. This conclusion is predicted by numerical simulations and has been validated by the NMR results. The confirmation that white-light illumination of optically dense samples generates a large isorhodopsin fraction casts doubt on the interpretation of some previous NMR data, purported to be studies of later photointermediates such as meta-I.[11,12] The possibility emerges that such data were actually obtained from the isorhodopsin photostate.

Bathorhodopsin may be generated preferentially by illumination with filtered short-wavelength light, which is absorbed well by isorhodopsin but relatively poorly by bathorhodopsin. However, only the outer layer of a rhodopsin-rich sample may be isomerized in a reasonable amount of time. In order to improve the bathorhodopsin yield, the solid particles of rhodopsin-rich material were mixed with glass beads to improve the light penetration. Interestingly a very sophisticated microstructure also occurs in the natural rod outer segment, where the membrane disks that are packed full with rhodopsin are separated by a thin aqueous layer. This construction is stabilized by a protein network[22] and the main purposes in this case probably is not optimization of light penetration, but to allow rapid diffusion of signal cascade components.

Acknowledgment. We thank BBRSC (U.K.) and Bruker Biospin for financial support. We thank H. J. M. de Groot and J. Lugtenburg for discussions.

Note Added in Proof. A recent paper (Coureux, P.-D.; Fan, Z. P.; Stojanoff, V.; Genick, U. K. *Structure* **2008**, *16*, 863−872) describes effects observed in a different photoreceptor protein which might conceivably be explained by light penetration phenomena of the kind described here.

Supporting Information Available: Complete ref 13. This material is available free of charge via the Internet at http://pubs.acs.org.

JA809878C

(22) Nickell, S.; Park, P. S. H.; Baumeister, W.; Palczewski, K. *J. Cell. Biol.* **2007**, *177*, 917–925.